OAK RIDGE NATIONAL LABORATORY
MANAGED BY UT-BATTELLE FOR THE US DEPARTMENT OF ENERGY

Light Water Reactor Sustainability Program:

Report Summarizing the Effort Required to Initiate Welding of Irradiated Materials Within the Welding Cubicle

Milestone M3LW-17OR0406012

June 2017

Light Water Reactor Sustainability Program

Report Summarizing the Effort Required to Initiate Welding of Irradiated Materials within the Welding Cubicle

Zhili Feng, Wei Tang, Jian Chen, Xunxiang Hu, Roger Miller, Brian Gibson
Materials Science and Technology Division

Allen Smith
Nonreactor Nuclear Facilities Division

Mark Vance
Office of Integrated Performance Management

Scarlett Clark
Fusion and Materials for Nuclear Systems
Oak Ridge National Laboratory

Gregory Frederick, Jonathan Tatman, Benjamin Sutton
Welding and Repair Technology Center
Electric Power Research Institute

Date Published: June 2017

Prepared under the direction of the
U.S. Department of Energy
Office of Nuclear Energy
Light Water Reactor Sustainability Program
Materials Aging and Degradation Pathway

Prepared by
OAK RIDGE NATIONAL LABORATORY
Oak Ridge, Tennessee 37831
managed by
UT-BATTELLE, LLC
for the
U.S. DEPARTMENT OF ENERGY
under contract DE-AC05-00OR22725

This page intentionally left blank

TABLE OF CONTENTS

This page intentionally left blank

LIST OF FIGURES

Page

This page intentionally left blank

LIST OF TABLES

Page

This page intentionally left blank

EXECUTIVE SUMMARY

The advanced welding facility within a hot cell at the Radiochemical Engineering Development Center of Oak Ridge National Laboratory (ORNL), which has been jointly funded by the U.S. Department of Energy (DOE), Office of Nuclear Energy, Light Water Reactor Sustainability Program and the Electric Power Research Institute, Long Term Operations Program and the Welding and Repair Technology Center, is in the final phase of development. Research and development activities in this facility will involve direct testing of advanced welding technologies on irradiated materials in order to address the primary technical challenge of helium induced cracking that can arise when conventional fusion welding techniques are utilized on neutron irradiated stainless steels and nickel-base alloys.

This report details the effort that has been required since the beginning of fiscal year 2017 to initiate welding research and development activities on irradiated materials within the hot cell cubicle, which houses welding sub-systems that include laser beam welding (LBW) and friction stir welding (FSW) and provides material containment within the hot cell. A significant installation effort has been required that includes implementation of the DOE approved safety basis supplement that covers irradiated materials welding at ORNL Building 7930; this installation effort is outlined within, along with ongoing research and development efforts in preparation for execution and post-weld characterization of irradiated material welds. Included within are updates regarding:

- Welding cubicle installation status
- Post-weld evaluation planning
- FSW process finalization
- LBW process finalization
- Software quality assurance process

Planning for post-weld evaluation has included an effort to identify a weld cutting method that can be implemented in-cell for creating metallographic specimens. An upgrade of a thermal desorption spectroscopy system for enabling the characterization of helium concentration of irradiated specimens is presented as well. The FSW process is being finalized on the fronts of tool evaluation and a software upgrade for enabling greater control of the FSW system, and initial LBW parameters have been selected based on an extensive modeling and experimental validation effort. Also covered is the software quality assurance process, which is relevant to the software that enables control of the remote welding subsystems in the hot cell cubicle. These aspects of facility and process development are nearing completion, which will allow for the initiation of research and development welding activities on irradiated specimens in the hot cell cubicle.

While welding is commonly used during nuclear reactor repair and upgrade activities, research conducted in this facility will address the need for identifying and validating advanced welding technologies capable of being used for repairs of highly irradiated material without helium induced cracking. This facility will be a significant asset for researchers and industry stakeholders alike, and research conducted within it will be critical in the effort to extend the operational lifetimes of existing nuclear power plants beyond 60 years of service.

This page intentionally left blank

1. Introduction

The advanced welding facility within a hot cell at the Oak Ridge National Laboratory (ORNL) Radiochemical Engineering Development Center, which will enable research and development of weld repair technologies for use on irradiated materials, is in the final phase of development. The development of this facility, the advanced welding capabilities it houses, and model materials on which initial welding trials will be performed have been jointly funded by the U.S. Department of Energy (DOE), Office of Nuclear Energy, through the Light Water Reactor Sustainability Program, and the Electric Power Research Institute (EPRI), through the Long Term Operations Program and the Welding and Repair Technology Center [1-5]. Research conducted in this facility will target the technical challenge of helium induced cracking in the weld repair of irradiated stainless steel and nickel-base alloys, addressing the growing need for weld repairs of degraded reactor internals that will be required for extending the operating lifetimes of existing nuclear power plants beyond 60 years of service.

This report summarizes the effort required from the beginning of fiscal year 2017 to enable the start of welding experiments on irradiated materials in the hot cell cubicle and provides extensive detail on these items:

- Welding cubicle installation status
- Post-weld evaluation planning
- Friction stir welding process finalization
- Laser welding process finalization
- Software quality assurance process

Installation of the welding cubicle, which provides material containment within the hot cell, has represented a significant effort, as has implementation of the DOE approved safety basis that covers welding experiments on irradiated materials at ORNL Building 7930. Post-weld evaluation planning is nearing completion, and weld specimen cutting for the creation of metallographic samples is discussed at length. Thermal Desorption Spectroscopy (TDS), which will be utilized for measurement of sample helium concentration, is also highlighted. Both friction stir welding (FSW) and laser beam welding (LBW) processes are being finalized in terms of parameter selection for initial trials, and additional items, such as the evaluation of FSW tooling, are presented here as well. Finally, the software quality assurance process, which is applicable to the software that enables control of remote welding equipment in the cubicle, is discussed.

2. Welding Cubicle Installation Status

Installation of the welding cubicle into Building 7930 Cell C and its supporting systems has required a significant effort in which several challenges have been overcome. Installation has involved repurposing remote manipulators for remote material handling, implementing a weld coupon transfer system between Cell B and Cell C, designing and building a work table that includes lead shielded storage, building a work table video system, upgrading the Cell B and Cell C interlock system, integrating the cubicle ventilation with the hot cell ventilation system, design and fabrication of service plugs, running permanent utility lines, implementation of the DOE approved safety basis supplement, and completing the software quality assurance process. The installation effort is in its final phase, and the effort to date has been completed within the constraints of a high work load at 7930 that includes support of the Pu238 Program, completion of Californium orders, RH-TRU waste pulls, PaR installation at Cell G, and Cave B Window/Liner/Glovebox installation.

The welding cubicle and adjoining workstation at 7930 required four manipulators. The current cost of manipulators from Central Research Lab is $140,000 each. To minimize the cost to the program, the facility repurposed two manipulators from 7930 and two that were salvaged from another facility. The two that were repurposed from 7930 presented little risk to program delay, but the two that were retrieved from salvage operations presented a high risk to program delay. This work was successfully completed however, and manipulators are awaiting final installation. Building 7930 utilizes a hydraulic rabbit transfer system to move irradiated items between the cells. The coupons that have been irradiated for initial welding R&D efforts are too large to be transferred through the system, which was identified at the onset of the project. To address this issue, extensions for the PaRs (remote material handling equipment) in Cell B and Cell C were installed, allowing coupons to be transferred between cells by different means. This issue initially presented a high risk to program delay, but has successfully been resolved. Building 7930 utilizes liquid filled shield windows to conduct/view remotely handled, in-cell activities. This project required two windows to conduct the activity; however, only one window was available at the cubicle position (the adjacent window at the work table position is filled with sand). To provide a new window would cost over $1M. To minimize the cost to the program, the facility purchased a video/camera system to conduct the coupon loading/unloading activity. Fabrication, testing, and checkout for this system (shown in Figure 1) are complete, and installation is scheduled for the week of June 26.

Figure 1: Testing of the work table video system

The 7930 hot cells have an interlock to prevent accessing the hot cells if a source of neutrons is present. The welding cubicle hazard will be gamma, which required that gamma detectors and associated interlocks be designed, procured, and deployed in the cells. Both the design and procurement are now complete, and installation is in progress with the end of July targeted for completion. To support loading

and unloading of coupons from the cubicle, a work station adjacent to the welding cubicle needed to be designed. Additionally, a lead shielded storage vault was incorporated into the table design. Fabrication, test, and checkout of the work station are complete, with installation scheduled for the week of June 26. Most of the ventilation components have been fabricated to tie the cubicle into the hot cell ventilation system. However, during cold weld testing, significant vibration was noted in the cubicle stand which required additional bracing. This bracing was installed but interfered with the existing ventilation design. This section was redesigned and fabricated, and installation is in progress. HEPA filter installation is scheduled for the week of June 26. Designs were finalized and fabrication is complete for the two service plugs that will be installed to connect Cell C to the control room/operating area. The service plugs are now awaiting installation. Permanent utility lines (e.g., argon, plant air, cooling water) were successfully run from the cubicle to the 3rd floor and operating areas.

An additional effort related to installation has been the implementation of the DOE approved safety basis supplement that covers welding research and development on irradiated materials in the cubicle. The completion of the software quality assurance process, which is relevant to the programmable logic controller software that is used to operate welding subsystems in the cubicle, is underway as well and is highlighted in detail in a following section of this report.

3. Post-Weld Evaluation Plans

Post weld evaluation plans for laser and friction stir welds on irradiated materials are being finalized. Welds will be created at ORNL Building 7930, where immediately upon completion, welds will undergo visual inspection using remote camera systems to search for indications of cracking or other irregularities, such as porosity. Any indications of defects found through visual inspection would guide subsequent welding in terms of parameter adjustments during the on-going welding campaign. At the completion of the welding campaign, welded coupons will be transferred to ORNL Building 3025E. A coupon traveler, currently under development, will also accompany each coupon to document every action that is taken, from welding through characterization. In the 3025E hot cells, welds will undergo another visual inspection that will include Dye Penetrant Inspection (DPI) to search for indications of cracks open to the top surface. Helium induced cracking is generally believed to be under-bead cracking that may or may not be open to the top surface, but DPI is a relatively quick test that could potentially generate meaningful results that could be fed back to researchers to inform the next welding campaign, instead of relying only on lengthy weld characterization work that will follow. Welded coupons will then be sectioned to extract metallographic specimens. Process-specific cut plans have been developed for laser welded coupons, which will contain up to four multi-pass welds, and friction stir welded coupons, which will contain one weld and include run-on and run-off tabs. Trial cutting of coupons is described in the following section of this report. Metallographic specimens will then be transferred to the Low-Activation Materials Development and Analysis (LAMDA) Laboratory in ORNL Building 4508. Specimens will be sized to both accommodate sample mounting capabilities at LAMDA and, more importantly, limit the specimen dose rate to below the LAMDA limit of 100 mR/hr/ft. Weld characterization activities in LAMDA may include, but not be limited to, further trimming or sectioning of specimens if necessary, sample mounting, grinding, polishing, optical microscopy to examine weld structure and identify cracking, focused ion beam (FIB) extraction of foils or atom probe tomography (APT) needles, transmission electron microscopy (TEM), thermal desorption spectroscopy (TDS) of base material to determine helium concentration, electron backscatter diffraction (EBSD) analysis, tensile bar machining and testing, and microhardness evaluation. Together these analyses will yield a comprehensive picture of the post-irradiation material properties, the impact of subsequent welding on microstructure and mechanical properties, and an assessment the ability of the advanced welding processes to make crack-free repairs on highly irradiated, helium containing materials.

3.1 Trial Cutting of Coupons

After welding (laser and friction stir) of irradiated material coupons in the cubicle at the hot cell, specimens will be cut from welded coupons for further investigation including quality evaluation, metallographic characterization, and mechanical properties examination. For cold material welded joint specimens cutting, various methods can be employed, such as band saw cutting, abrasive saw cutting, slow saw cutting, and wire electrical discharge machining (EDM). However, irradiated material specimen cutting method is limited by many factors, including coupon radiation dose rate, facility allowance, and equipment availability. For example, the abrasive saw cutting is a very powerful and fast cutting method, but sparks during the cutting may cause a fire hazard in the hot cell. The objective of this work was to identify the proper method for future irradiated material welded coupon specimen cutting in the hot cell, evaluate the cutting efficiency and quality, and provide initial input regarding machine modification to allow for utilization in the hot cell, using unirradiated 304 stainless steel (304 SS) as dummy coupons. In this work, slow saw, wire EDM, diamond wire, and band saw cutting were tested and evaluated.

3.1.1 Slow Saw Cutting

Slow saw cutting is always the first choice for small size specimens requiring precise and high quality cutting. A previous experiment showed that a corner of area approximately 0.5 inch x 0.35 inch could be cut off easily from a 304 SS specimen using a slow saw; the cut coupon is shown in Figure 2.

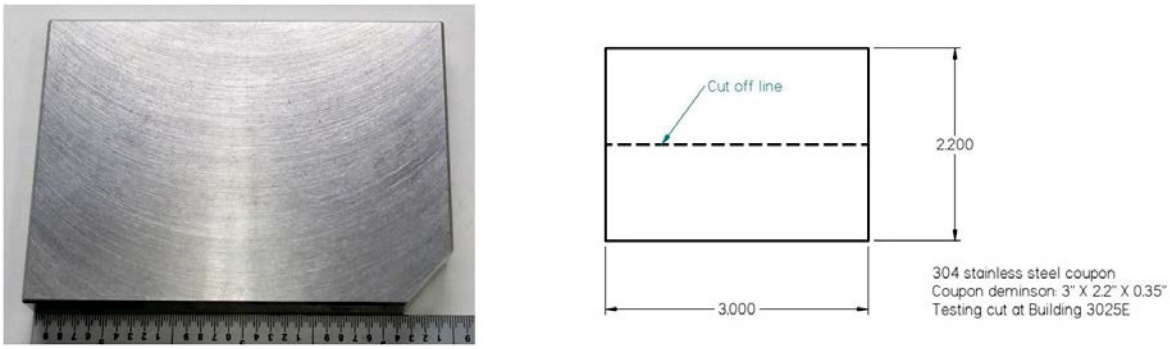

Figure 2: Coupon corner cut by a slow saw (L), Slow saw test cut plan (R)

Therefore, the first test cut trial was performed on the same slow saw cutting machine. Comparing with the previous coupon corner cut off, the test cut worked along a longer cutting line and cut through a larger area on a piece of unirradiated 304 SS dummy coupon, whose dimensions were 3 inch x 2.2 inch x 0.35 inch and is shown in Figure 2. The designed test cut was along the 3 inch dimension, and the total cutting area was 3 inch x 0.35 inch.

To perform the test cut, a 4 inch diameter, 0.025 inch thick Malco high speed steel jeweler's slotting saw was used with a slow cutting machine; the machine setup is shown in Figure 3. After about an hour of cutting, the saw blade was worn and stopped cut further into the 304 SS coupon; see Figure 3 for the worn saw blade. Later, a new saw blade was used to replace the worn one to continue the cutting procedure. However, it was quite difficult to align the new saw blade with the original cut on the coupon because of the machine's loose design and material deformation by residual stress release; hence, significant saw vibration was observed during the continued cutting process. To avoid any damage to the saw, a fresh cut was started with the new saw blade but it couldn't cut through the whole cross section either.

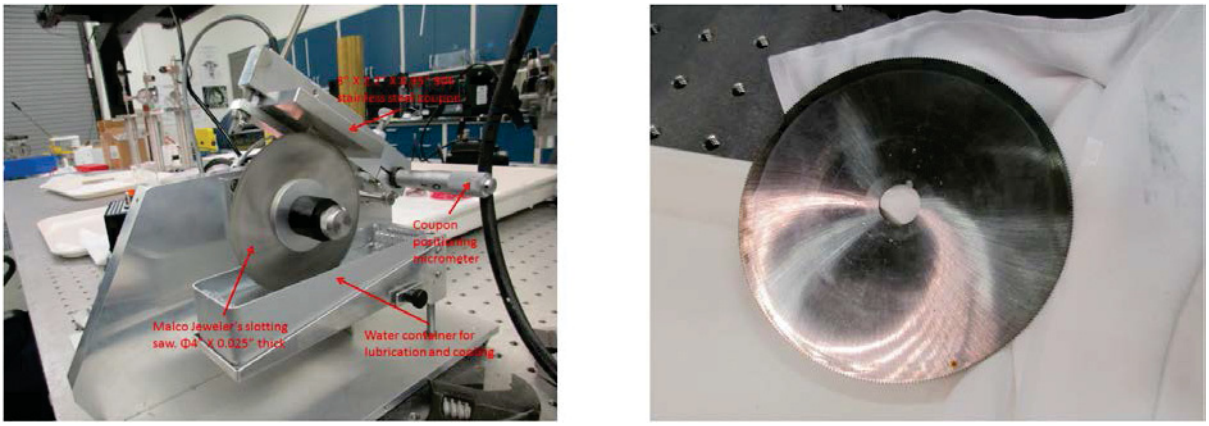

Figure 3: Slow saw test cut setup (L), Worn jeweler's slotting saw blade (R)

In summary, by using the high speed steel jeweler's slotting saw, small area such as 0.5 inch x 0.35 inch of 304 SS specimen can be cut off easily. A slightly larger area specimen may also be cut off easily. However, if the cutting specimen area is relatively large, such as 3 inch x 0.35 inch demonstrated in the trial, the high speed steel jeweler's slotting saw is not capable to finish the cut. Possible reasons for that include the saw not being designed for large area, tough material cutting and the machine not being powerful enough to complete the cutting.

3.1.2 Wire Electrical Discharge Machining

EDM is a manufacturing process that employs electrical discharges (sparks) to machine a desired shape of materials. Wire EDM uses a thin single-strand metal wire, usually brass, as the carrier, to feed and cut through the workpiece, and the process is carried out in a tank filled with dielectric fluid, typically deionized water. A wire EDM machine and its working part are shown in Figure 4. The wire EDM machine is relatively expensive with high maintenance. It can perform precision cutting with fast speed, but the brass wire is a consumable material. Considering the cost of the machine, the maintenance, and the post-cutting consumables handling and disposal with respect to radiation contamination, wire EDM will not be used as the specimen cutting method at this time.

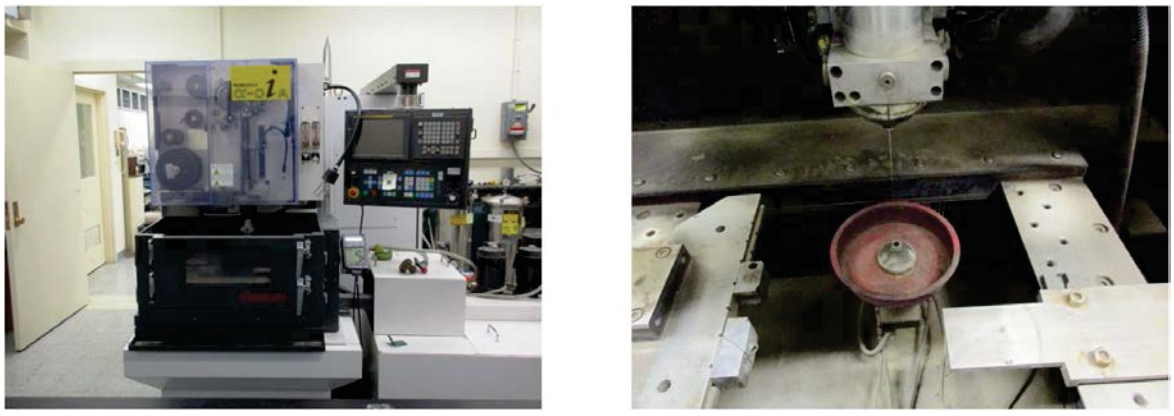

Figure 4: Wire EDM machine (L), Wire EDM close-up (R)

3.1.3 Diamond Wire Saw Cutting

Diamond wire saws produce smooth, sharp-edged surfaces on virtually any material. The "cutting tool" employs a stainless steel wire with diamonds embedded into its surface. A diamond wire saw machine is shown in Figure 5. To evaluate the diamond wire saw cutting, a 304 stainless steel coupon with the dimension of 2.25 inch x 0.75 inch x 0.385 inch was used as the dummy sample. The detailed setup and the wire status during cutting are shown in Figure 5. From Figure 5, it is clear that the diamond wire is bent by the feeding system, cutting in more at the two edges of the coupon and less at the center part of the coupon.

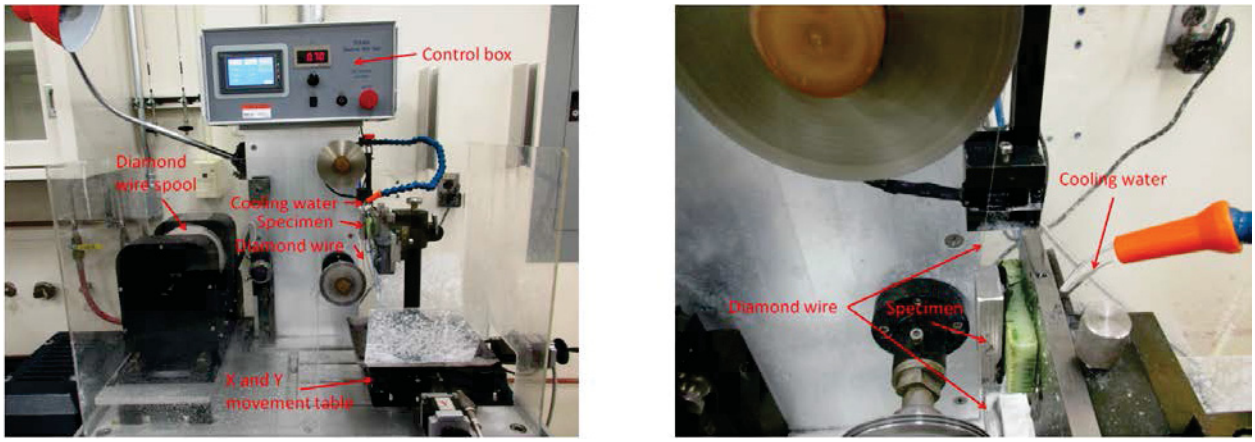

Figure 5: Diamond wire saw machine (L), Diamond wire cut of 304 SS coupon (R)

With this specific diamond wire saw, the cut in distance at the coupon two edges was about 2 mm after one hour of running, see Figure 6 for details, but the middle part of the coupon only had some surface scratches, see Figure 6 for details. In summary, diamond wire saw can perform precision cut with excellent surface finish on materials, but the cutting speed is very slow. Moreover, the change of the diamond wire when it is worn is quite complicated and tedious, which may be very difficult to perform by the manipulator in a hot cell.

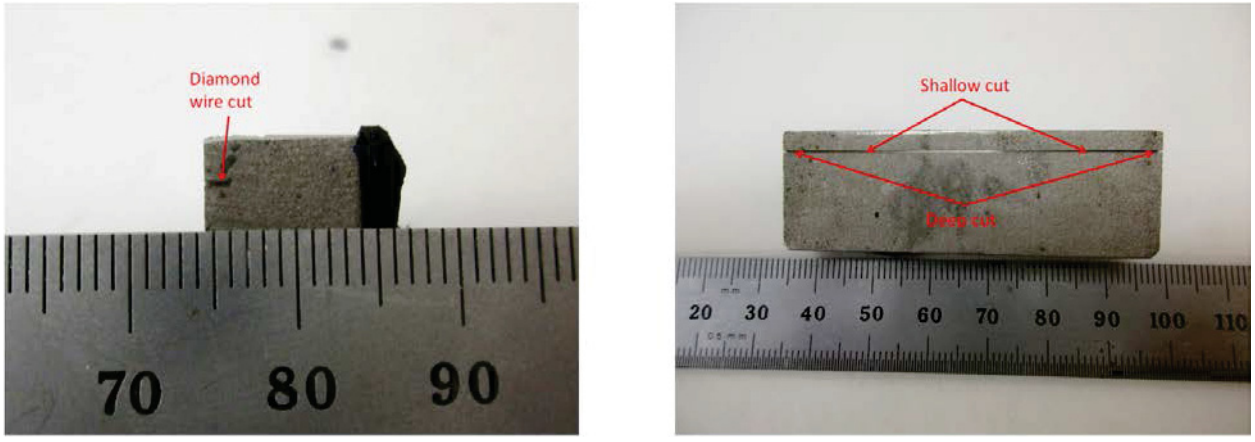

Figure 6: Cut specimen side view (L), Cut specimen top view (R)

3.1.4 Band saw cutting

A new band saw machine, which price is much lower than a brand new slow saw machine, was purchased and is shown in Figure 7. It contains a motor, a press switch mounted on the handle, a vise mounted on the base, and a guard with a band saw enclosed. The cutting process is implemented by holding the handle, moving the saw blade close to the coupon, pressing the switch to turn on the machine, and applying pressure to the coupon. The setup of the band saw test cut is shown in Figure 7 also.

Figure 7: Band saw for coupon cut (L), Coupon setup with the band saw (R)

It took the band saw about 3 minutes to cut through the 304 stainless steel coupon, and the cutting area was about 2.2 inch x 0.35 inch; see Figure 8 for the coupon after the cutting. During the cutting process, no lubricant or coolant was applied. In addition, the cut surface produced by this band saw machine is much smoother than that cut with a regular lab scale band saw; see Figure 8 for the comparison. The smooth cut surface will benefit the specimen metallographic preparation later.

Figure 8: 304 stainless steel cut coupon (L), Test cut surface comparison (R)

The feasibility of using a band saw to cut specimens out from stainless steel coupons has been demonstrated. With some further modifications, this machine is expected to be used in the hot cell for irradiated material specimen cutting. In addition, the clamping system also needs to be modified so that thin specimens can be sliced from the coupon. The band saw test cut of regular 304 SS coupon satisfied the time and quality requirements for specimen preparation. Therefore, it is possible to use the band saw

to cut specimens to the final size for metallographic characterization and mechanical testing, instead of using band saw for rough cut and slow saw for precision cut. It is also noticed that the saw blade used for this test cut was a general type. We will check if there is any special saw blade for stainless steel cut available and will test the special saw blade when we get one. The saw blade changing frequency and procedures will be evaluated as well. In addition, coupon temperature during the saw cutting will be measured and using lubricant and coolant during the cutting will be reviewed.

Comparing all four specimen cutting methods evaluated and tested in this work, the band saw is capable to cut through a relatively large 304 stainless steel coupon with short time, smooth finish, and low cost. Further modifications are needed to install and use a band saw machine in a hot cell for irradiated material specimen cutting.

3.2 Thermal Desorption Spectroscopy

Thermal desorption spectrometry (TDS) is a powerful tool to investigate gas behavior in nuclear materials research, aiming to observe gas desorption flux in steady/transition state from a sample when the sample is being heated. Conceptually, TDS is straightforward: through a direct contact heating method the material is heated with the desorbed gas being measured. This technique is critically dependent on the ultra-high vacuum ($<10^{-9}$ torr) capabilities of the system to reduce the influence of background. A new TDS system, coupled with an in-situ 20keV noble gas feeding ion gun has been established in LAMDA lab at ORNL.

This ultra-high vacuum system, as shown in Figure 9, consists of three major functional chambers, i.e., implantation chamber, heating chamber, and measurement chamber. Each of these three chambers is equipped with a Pfeiffer turbo-drag-pump, of which the pre-vacuum is obtained by the deployment of Varian TriScroll 600 oil-free dry scroll vacuum pump.

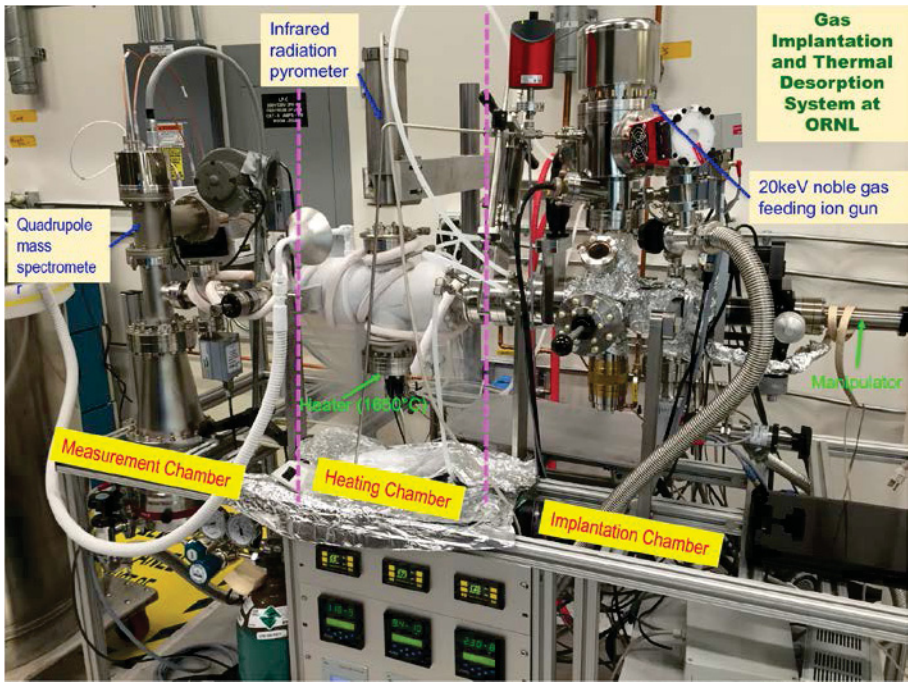

Figure 9: The gas implantation and thermal desorption system in LAMDA lab at ORNL

The targeted pressure level of this system is at a level of 10^{-10} torr. Due to the large volume of the measurement chamber and the fact that fast pumping rate is necessary when thermal desorption measurement is performed, a more powerful turbo pump (Pfeiffer HiPace 700 turbo-drag-pump, 680 l/s) is applied for the measurement chamber. The other two chambers are pumped by using Pferiffer HiPace 80 turbo-drag-pumps (71 l/s). The pressure levels of the chambers are monitored by three MKS 909AR digital and analog hot cathode vacuum transducers.

After being placed in the tungsten crucible, the sample will be transported by a MDC special precision magnetically coupled transporter, mounted onto a DualAxis XY stage, from implantation chamber to heating chamber by passing through the connecting vacuum channel. The old electrical resistivity heater was designed and manufactured by HeatWave Labs, with a maximum temperature of 1150°C.

Helium detection in the TDS is preformed by using a Pfeiffer HiQuad quadruple mass spectrometer equipped with a Channeltron type electron multiplier. A linear relationship exists between ion current in the mass spectrometer and helium partial pressure:

$$I(A) \propto P_{He}(torr). \tag{1}$$

The helium desorption rate from a sample is described by:

$$L(t) = \frac{k_B T}{V}\left(\frac{dN}{dt}\right) = \frac{dP(t)}{dt} + \frac{S}{V}P(t) = \frac{dP(t)}{dt} + \frac{P(t)}{\tau}, \tag{2}$$

where $L(t)$ is the helium desorption rate, N is the number of helium atoms, $P(t)$ is the partial pressure of helium, S is the pumping speed (L s^{-1}), V is the chamber volume (L), and $\tau = V/S$, the pumping time constant (s).

The TDS system can operate in two modes, either a static or a dynamic mode. In the static mode, the $P(t)/\tau$ term in Eq. (2) is minimized, with no pumping on the measurement chamber. In the dynamic mode, the $dP(t)/dt$ term in Eq. (2) is minimized, and τ is adjusted by the valve to the turbo-drag pump. This system operates in the dynamic mode.

The mass spectrometer will be calibrated by a standard helium leak to determine a calibration factor:

$$Q = \#He\ atoms / I \tag{3}$$

Then the desorbed helium amount could be determined.

In order to obtain the total amount of helium generated through transmutation reactions in the studied B-doped 304L and 316L alloys, the heater needs to be upgraded to reach a maximum temperature of 1650°C, which is high enough to melt the materials of interest and enable the full release of contained helium. The design and fabrication of the new heater was completed by Materials Research Furnaces Inc. in 2016. Figure 10 shows the schematic plot of this customized heater.

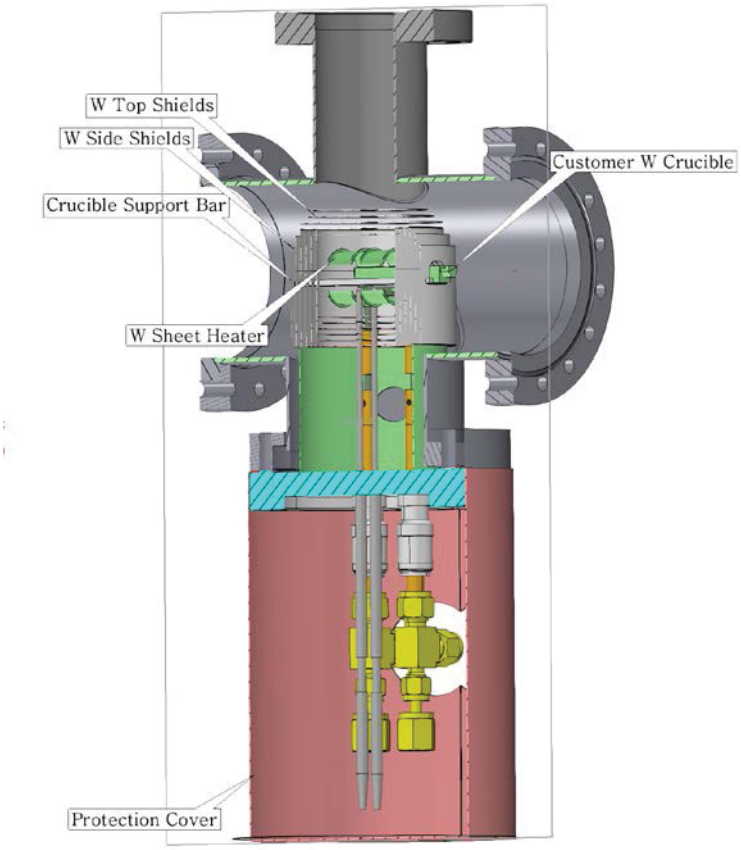

Figure 10: Schematic plot of the new heater together with the TDS measurement chamber

The W heating element is used to build the hot zone, where a W crucible support bar is inserted in. To improve the heating efficiency, W and Mo radiation shields surrounding the work area and the heating element are applied. The open window on the shields provides access for loading and unloading crucible. Two Type-C thermocouples (one control and one over-temperature protection) with direct access into hot zone are used. A 3kW rack mount DC power supply are connected with the two water-cooled power feed through by the double insulated water-cooled power cables. One Eurotherm 3504 temperature programmable controller and one 3216 over-temperature limit controller are used control the temperature ramping process.

To accommodate the new heater, the utilities for the TDS system at LAMDA have been modified. 208V, 3-phase, 60 Hz power is needed and the water-cooling used for the heater requires 0.75 GPM flow with an inlet temperature of 70°F and 50 psi. The construction of the required utilizes has been completed in February 2017. This new heater was successfully installed and tested in April 2017. Figure 11 shows the recorded temperature readings from the type-C thermocouple as well as the set values during a linear temperature ramping process with a ramping rate of 0.5K/s. The temperature control is excellent when the temperatures are in the ranges of RT~ 1000K and 1051~1900K (although the maximum temperature shown in Figure X is 1673K). The fluctuation of the actual temperature from 1000K to 1051K was observed due to the transition of the two sets of PID controlling parameters. The fluctuation range will not impact the final helium determination since the ultimate temperature to be reached will be greater than 1700K. A recent testing shows that the new heater could be stably running at 1900K for 0.5 hours, which is high enough to melt the samples of interest.

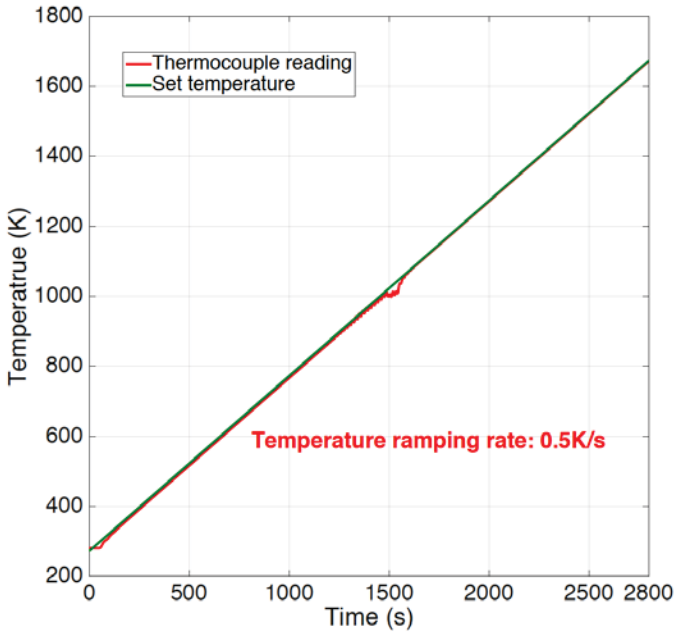

Figure 11: Temperature control during a linear ramping process with a ramping rate of 0.5K/s

In order to align with the heater upgrading, a new W crucible with a small cap, avoiding sputtering of molten materials, was designed as shown in Figure 12. The new crucibles were fabricated by Midwest Tungsten Service, also shown in Figure 12.

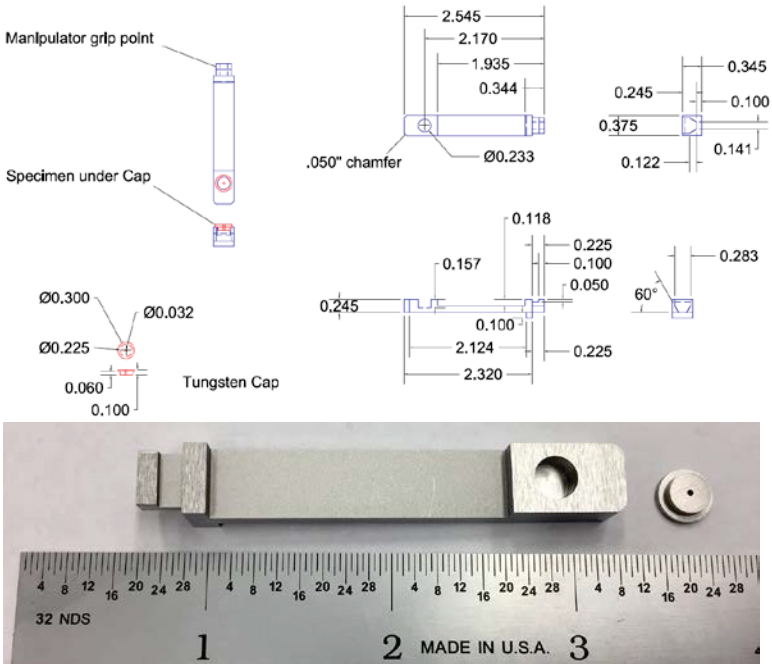

Figure 12: Design (top) and photo (bottom) of the new W crucible with cap to fit the open access of the radiation shields

A critical factor impacting the measurement accuracy is the clean background, indicated by the ultra-high vacuum. In this study, helium is the element to be determined. Therefore, extremely low helium partial pressure in background during the temperature ramping process is desired. Background signals have been recorded to verify the detecting limit of this system. Figure 13 shows the mass spectrometer outputs of three important elements, i.e., He, H_2, and H_2O, during the temperature ramping process shown in Figure 11. It is evident that the signal of helium is always in a low level, less than 5×10^{-13} Amp. By applying the conversion coefficient obtained from the calibration process by using the VTI standard helium leak, this electrical current is equivalent to 2.01×10^{10} He atoms/s.

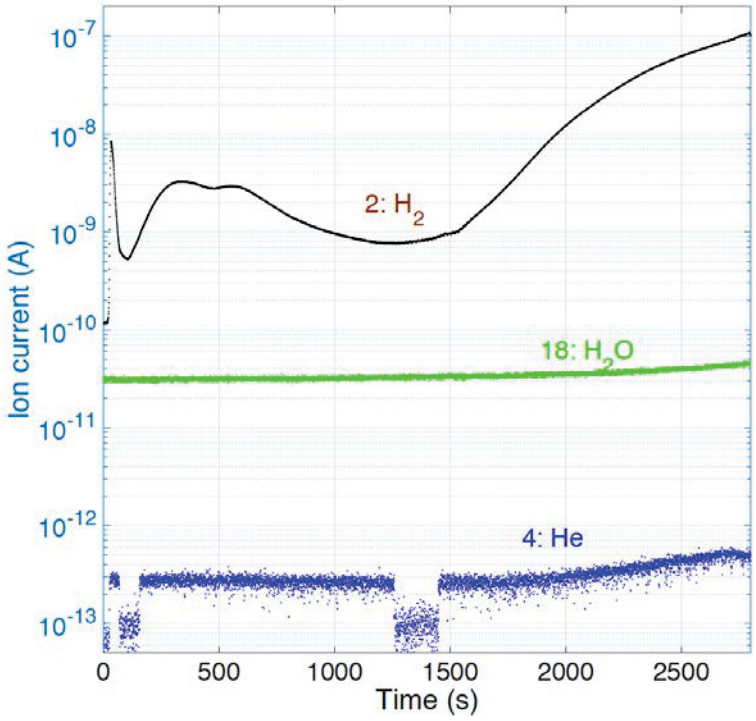

Figure 13: Mass spectrometer signals of He, H_2, and H_2O during the temperature ramping process shown in Figure 11

Note that this background testing was performed without the presence of crucible. The newly-fabricated W crucibles need to be annealed to remove the possible remaining on the surface to maintain the clean background at high temperature. Four sets of W crucibles and caps have been annealed at 1600°C and ready for the real sample testing. However, the TDS system is experiencing a mass spectrometer failure. The mass spectrometer has been sent back to the vendor for repair. Once it is returned (expected by the end of June), sample testing will be started.

4. Friction Stir Welding Process Finalization

The FSW process is being finalized prior to welding irradiated materials on two fronts: FSW tool wear has been evaluated to determine the tool life that can be expected during irradiated material welding campaigns, and software modifications on the hot cell FSW system are underway that will enable a greater level of control regarding tool-workpiece engagement in the z-axis during the welding process.

4.1 Friction Stir Welding Tooling

A study was undertaken that was aimed at characterizing tool wear of the Polycrystalline Cubic Boron Nitride (PCBN) FSW tools that will be used in the welding cubicle to determine the number of standard sample configurations (run-on tab, irradiated coupon, and run-off tab) that could be welded without volumetric defects resulting from tool wear arising. This study was carried out on an instrumented FSW test bed using unirradiated, representative 304 stainless steel samples, and analysis of the collected data was recently completed. Tool wear and resulting weld quality were evaluated through multiple post-weld analyses that included laser profilometry, weighing, radiographic non-destructive evaluation (NDE), and metallographic sectioning. Measurements of tool geometry were made in-situ and ex-situ using a Keyence LJ-V7080 laser profilometer. Through this characterization, the useful life of the PCBN tooling for producing defect-free welds with this combination of material, sample configuration, and welding parameters was successfully determined. Profilometry measurements yielded mid-plane 2D traces, point measurements at locations of interest, area measurements at the mid-plane, and 3D maps of tool wear. Figure 14 displays an example of a 3D tool wear map alongside tool images.

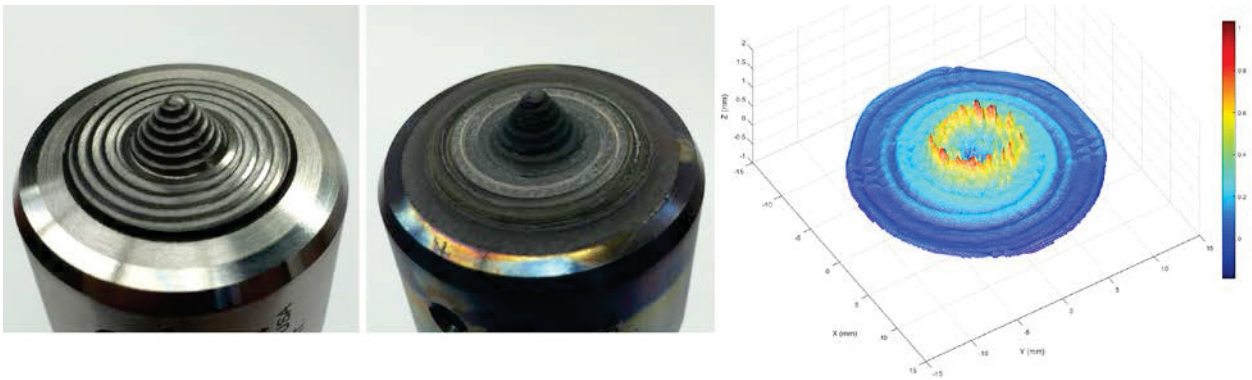

Figure 14: FSW tool (from L to R): Tool in new condition, Tool after 12 welds, Z-axis wear after 12 welds as determined through ex-situ laser profilometry

It was found that measurements of tool geometry could be correlated to defect formation, and an interesting observation was that the measurement of probe length decrease was not necessarily a good indicator of overall wear. Limited mass measurements confirmed that weighing is a viable method for quantifying tool wear as well. Post-weld x-ray NDE successfully detected volumetric defects once defect size was adequate; these results were compared against defect observations in the metallographic cross-sections. An additional aspect of this study was that collected weld forces (torque, traversing force, and side force) were examined in an attempt to correlate observations in the force data with tool wear or defect formation to evaluate the potential for remote, in-process monitoring. An interesting initial observation was that the as-collected torque magnitude increased from weld to weld somewhat counterintuitively, perhaps due to plunge depth increases under axial force control as wear occurred and thus slightly greater engagement of the extents of the tool shoulder with the workpiece, or a change in the area over which shear flow stress was applied due to gradual removal of the tool features. Weld forces also displayed periodicities that the literature would indicate could correspond to material flow characteristics and defect formation. As such, the frequency components of the weld forces were computed and examined, and there was evidence of variation in the spectral content as the tool experienced wear and defects began to form. A multilayer perceptron, a type of artificial neural network, within inputs of power spectral density across a range of frequencies and a logical output was trained and evaluated as a means of pattern recognition and classification of weld quality. Inputs derived from torque

were initially the focus due to the limited instrumentation of the friction stir welder in the advanced welding cubicle; the spindle motor current signal is available, which has been used as an indirect measurement of torque in the literature. Adding inputs derived from the planar forces (either the traversing or side force) yielded improved performance and showed that this methodology was viable for enabling in-process monitoring of FSW of stainless steel. These results are the subject of a manuscript that has been accepted for publication [6] and have allowed for a significantly better understanding of the tool wear characteristics than can be anticipated during weld repair trials on irradiated materials in the cubicle, enabling detailed planning of future tool usage.

With respect to future tool usage, the economics of FSW tooling options were examined to evaluate the relationship between tool life and cost for tools that are capable of welding higher melting temperature alloys. This will allow for the planning of long term tool usage in the research and development welding of irradiated materials in the hot cell cubicle. Since FSW was invented, many materials, mainly hardened metals and nonmetals, have been evaluated and ultimately selected for use as FSW tool materials. A summary of these FSW tool materials is listed in Table 1.

Table 1: FSW tool materials for joining various materials [7]

Material Characteristic	Tool Material Class				
	Tool steels	Superalloys	Refractory metals	Carbides, cermets, and ceramics	Superabrasives
Room-temperature strength	Good	Excellent	Excellent	Excellent	Excellent
Process-temperature strength	Good	Very good	Excellent	Good	Excellent
Chemical inertness	Good	Very good	Good	Good	Excellent
Wear resistance	Good	Good	Very good	Good	Excellent
Fracture toughness	Very good	Very good	Very good	Good	Poor to good
Availability	Excellent	Very good	Very good	Very good	Very good
Cost	Excellent	Very good	Poor to acceptable	Good	Poor to acceptable
Examples	H13, O1, D2, etc.	Cobalt and Nickel-based	Molybdenum and tungsten-based	Cemented tungsten carbide	Polycrystalline cubic boron nitride (PCBN)

From Table 1, it is clear that the FSW tool materials include several types of metals and nonmetals, from regular tool steel such as H13 or O1 to superabrasives such as PCBN. Different types of materials have different properties, machining ability, availability and cost, and can be applied in different materials joining. Soft materials such as aluminum alloys can be joined by any material listed in Table 1, and tool steel is always the right choice because of its good machining ability and low cost features. On the

contrary, when hard and high temperature materials such as stainless steels or nickel alloys are to be joined by FSW, tool steel is no longer the right choice for the tool, and they are limited to a few types of materials, which own higher hardness and wear resistance than tool steel at elevated temperature.

Compared with soft materials like aluminum FSW, stainless steel and nickel alloy FSW are much more difficult to perform because of much higher welding temperature (~1000 °C vs. ~500 °C or less) and flow stress. Consequently the tool faces much more severe working conditions during FSW. As a result, most researchers chose refractory materials, carbides, ceramics, or superabrasives as the tool material. Advantages and disadvantages of those three types of materials for FSW tooling are shown in Table 2.

Table 2: Characteristics of tool materials for FSW of high temperature alloys

Material Type	Characteristics
Refractory metals	• Acceptable price (except W-Re), and the price is also dependent on material quality • Difficult to machine, especially for fine features, but simple geometries can be machined • Fine features on refractory metal tools tend to wear quickly
Carbide, cermets and ceramics	• Very reasonable price • Lower high temperature durability than the other two materials • Difficult to machine, but simple geometries can be machined
Superabrasives	• Expensive • Fine features can be managed to put on • Quite challenging in terms of re-machining • Relatively low wear rate and fracture toughness

A thorough search of academic publications showed that the most common tool material used for stainless steel FSW are tungsten alloys and superabrasive PCBN, with tungsten–carbide being adopted the most because of its inexpensive price, but it tends to have low durability and wear resistance under high temperature and high stress conditions. On the other hand, tungsten-rhenium alloys and PCBN are quite expensive, but their durability and wear resistance under high temperature and high stress conditions are excellent. These characteristics enable the following conclusions to be drawn regarding future tool usage:

1. All FSW tool materials for stainless steels and nickel alloys are difficult to machine, and detailed features may not be able to be put on by conventional machining.
2. PCBN is the best tool material for stainless steels and nickel alloys regarding room temperature strength and high temperature strength and wear resistance, but the cost is very high. For the application of FSW of nuclear structural materials, boron deposition in the workpiece as the tool wears could be an issue.
3. Refractory materials such as W-Re are good for stainless steels and nickel alloys, and tungsten remaining in the stir zone due to tool wear may not be an issue in the nuclear structural welding application; however, new procedures would have to be carefully scrutinized to account for tools with fewer features and to monitor tool life.
4. Carbides, cermets, and ceramics are quite inexpensive compared with the two materials above, but their durability and wear resistance at high temperature may be unacceptable.

4.2 Friction Stir Welding Software Modification

At the direction of EPRI and ORNL, Dynamic Design Solutions (DDS) Inc. designed and produced the FSW machine inside the cubicle. This machine will be used to friction stir weld irradiated materials with different helium levels, and goals are to investigate heat input effects of irradiated materials welding, and produce repair welds without defects initiated by helium accumulation, such as voids and cracks, which always appear during traditional fusion welding of irradiated materials. To accomplish a basic FSW procedure, there are three major motions that the FSW machine needs to achieve, spindle rotating, spindle or table moving up and down, and spindle or table moving along the welding direction (X direction). The current FSW machine can achieve all motions listed above, and the control software interface is shown in Figure 15, where the researcher may input FSW control parameters.

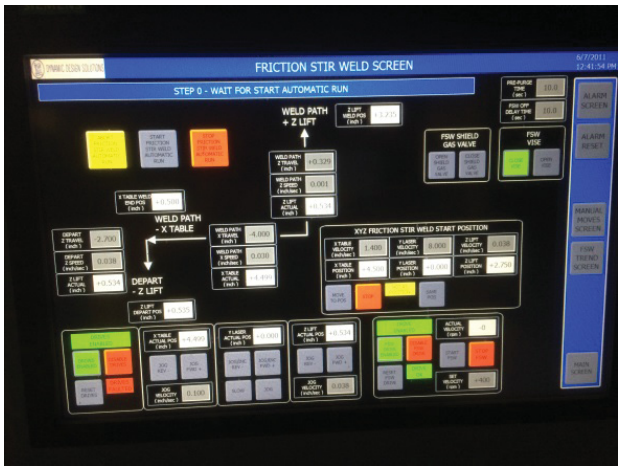

Figure 15: FSW control software interface

The feasibility of FSW inside the cubicle using the machine designed and produced by ORNL, EPRI and DDS has been demonstrated, and a FSW process is shown in Figure 16, where movements of the X and Z direction were accomplished by the table underneath the spindle head.

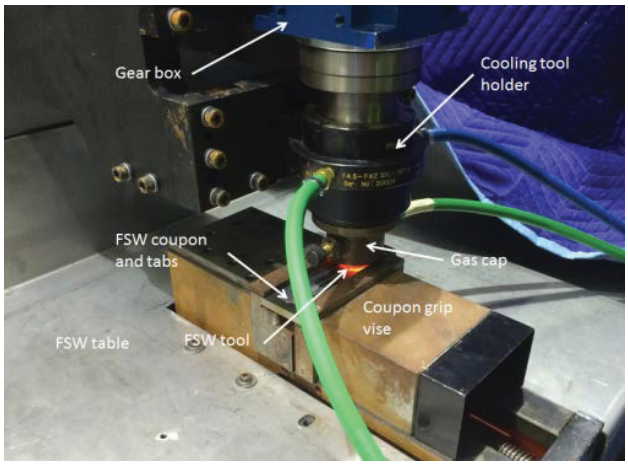

Figure 16: FSW process in the cubicle

To execute a FSW process, the researcher may input all FSW control parameters including tool rotational speed, plunge in depth (Z direction), traveling speed, and traveling distance (X direction) at the control interface shown in Figure 15, then move the table with a coupon clamped on to the starting position, and run the machine. A FSW coupon produced by this machine with a proper-controlled program is shown in Figure 17.

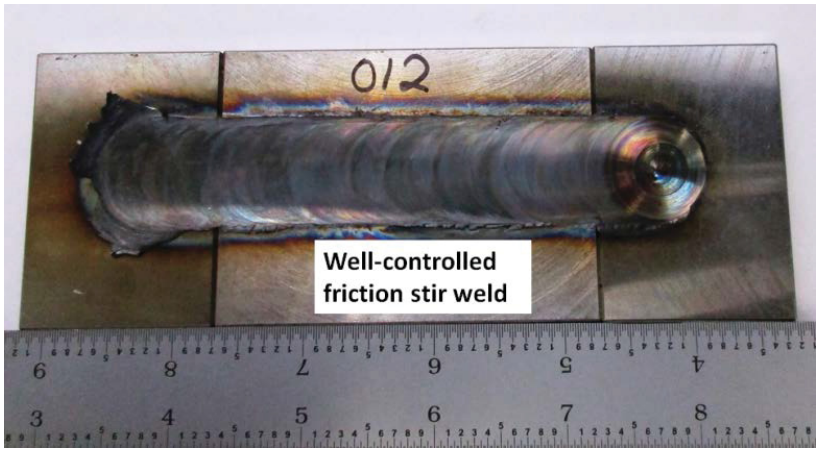

Figure 17: Friction stir weld produced by a properly-controlled program

The way of the current control software design allows the researcher to program and run the FSW process easily, however, after the FSW machine starts to run, the control software does not allow the researcher to have any interaction with the FSW machine or the FSW process, except the emergency abort/stop. In some cases, this lack of interaction/adjustment during the FSW process may result improper control and defective weld, such as the weld shown in Figure 18. During that FSW process, the initial inputted tool plunge in depth was slightly lower than the optimum value, which resulted contact area of the tool and the material turned quite small at the end of the process, and caused a surface defect at the end of the weld. This welding defect can be avoided if the researcher can adjust the table position during the FSW that allows the tool plunge in more by the end of the FSW process.

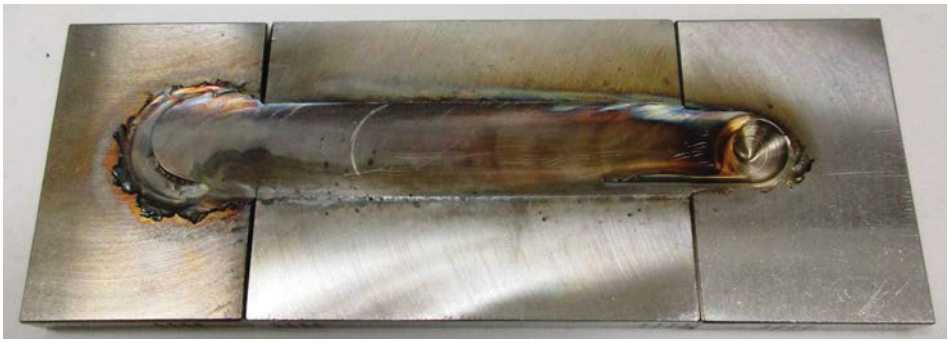

Figure 18: Friction stir weld with surface defect near end

In order to have better control of the FSW process, two major control software modifications were requested from ORNL to DDS, after the FSW machine initial running and evaluation:

- The current control software only allows inputting one set of FSW parameters input in a single process. Modification will be made to allow the researcher inputting multiple sets of FSW parameters in a single FSW process.

- The current control software does not allow any parameters adjustment during the FSW process, except emergency abort/stop. Modification will be made to allow the researcher adjusts the FSW parameters during the FSW process, such as let the tool plunge in more or less, step by step, if it is necessary.

Details of the modification have been discussed with DDS and EPRI. Once the software modification is completed at DDS and the hot cell is available at ORNL, the DDS programmer will come to ORNL to install and test the modified control software.

5. Laser Welding Process Finalization

Toward the goal of developing an advanced LBW technology for enabling weld repair of irradiated reactor components, a new in-situ stress management approach for controlling temperature and strain distribution around the weld pool was developed. The in-situ temperature and strain distribution were measured by digital image correlation (DIC) and infrared (IR) thermography respectively. In addition, a computational finite element (FE) model that can be used to gain a fundamental understanding of the effect of welding stress and temperature on the formation helium induced cracking during welding, and the effect of the auxiliary heating on stress and temperature distribution was developed. It is noted that the technology developed in this task is under patent application. As such, specific details in the technology are omitted. Nevertheless, the effectiveness of the proactive in-situ stress management technology is illustrated.

As shown in Figure 19, the multi-beam laser welding system consisted of a primary laser head used for welding and a galvo-scanner for auxiliary heating. The welding and auxiliary laser heads were powered using two separate IPG fiber laser power supplies. At the optimal working distance between the optical lens and the base plate, the galvo-scanner was capable of delivering a laser beam at any point within an approximate 10-inch square region with a scanning speed up to 3 meters per second.

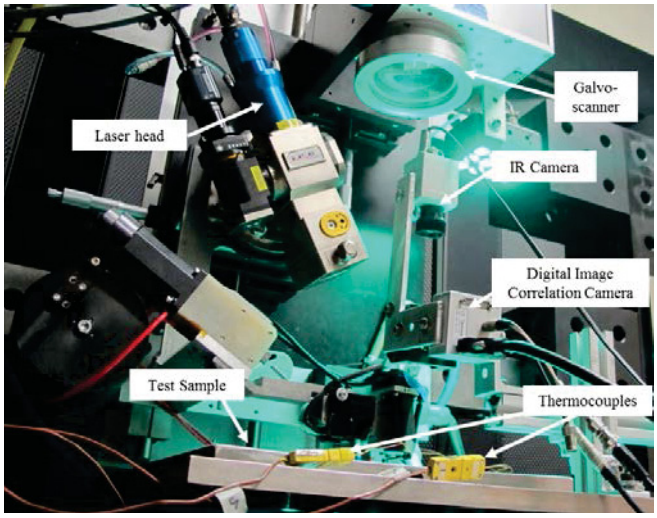

Figure 19: Multi-beam laser welding system for in-situ strain and temperature measurement

A schematic of the auxiliary beam scanning pattern behind the weld beam is provided in Figure 20. The beam is rapidly scanned back and forth on both sides of the center line along the path (B-A-B and jumped to C-D-C). The dimension of the scanning pattern and distance from the weld centerline was optimized by a large amount of experimental and numerical trials.

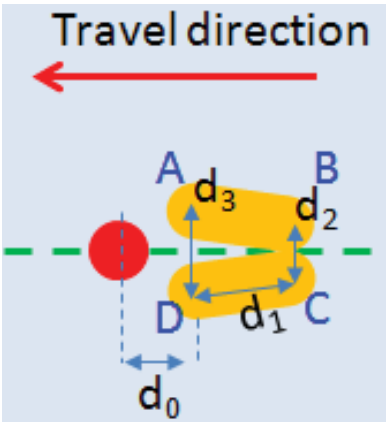

Figure 20: Auxiliary beam alignment and scanning pattern behind the primary weld laser beam

This study on stress reduction by multiple laser beams mainly focused on single-pass welds. The influence of multi-pass welds is still under investigation. To demonstrate the effectiveness of stress reduction on single-pass welding, two bead-on-plate welds were performed on stainless steel (grade 304L) base material with 308L filler material addition. Welding travel speed was 11.4 mm/s. Argon was the shielding gas to protect the weld. The test samples were welded on a backing plate to minimize distortion (an example test plate is shown in Figure 21). Laser welding parameters in the cases with and without auxiliary beam, as well as scanning pattern parameters, are listed in Table 3.

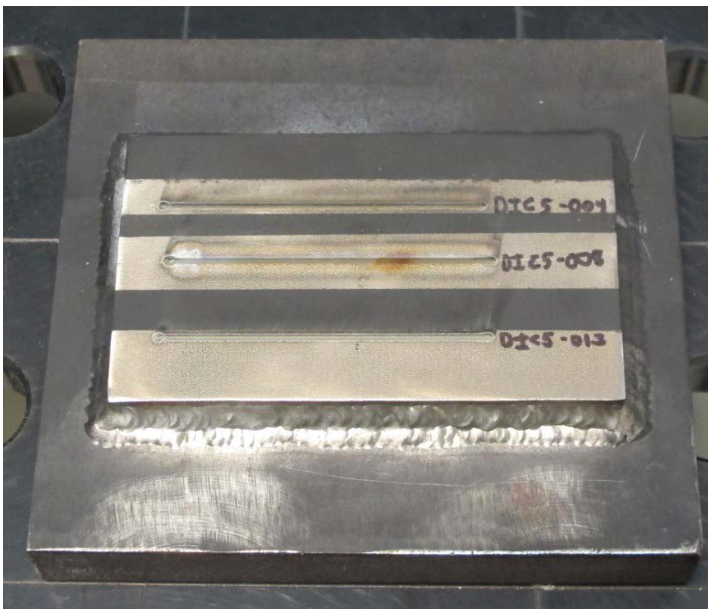

Figure 21: Example 304L stainless steel test plate welded to a rigid carbon steel backing plate

Table 3: Laser welding parameters and scanning patterns

Case #	Weld Power (Watts)	Scan Power (Watts)	Travel Speed (in/sec)	Wire Feed Speed (in/min)	d0 (mm)	d1 (mm)	d2 (mm)	d3 (mm)
no aux. beam	1000	0	0.45	75	-	-	-	-
Pattern a	1000	2000	0.45	75	3	5	6.5	6.6
Pattern b	1000	2000	0.45	75	3	8	6	3
Pattern c	1000	1200	0.45	75	3	5	5.5	5.6

Numerical models were used to assist in the development of the new welding process since the stresses could not be directly measured. To benchmark these numerical models, the evolution of both strain and temperature adjacent to the weld bead was measured during the experimental tests (i.e., in-situ). The strain field was measured during the experiments by means of the digital image correlation (DIC) technique. It is noted that the conventional DIC strain measurement requires a painted speckle patterns on the surface and a stable illumination source [8]. This is challenging for in-situ welding applications because the high temperature of welding may damage the painted speckles and the intense laser plume acts as an unstable and moving illumination source. To address these issues, a newly developed high-temperature DIC method [9] including a high-temperature resistant speckle preparation method and a special optical illumination and filtering system was applied in the measurements. During welding, a digital camera is used to detect distortion in the speckle pattern, and was positioned nearly perpendicular to the sample surface. Following welding, the image sequence was post-processed by VIC-2DTM to calculate the strain. The thermal field was simultaneously measured by an infrared (IR) camera. Because the surface emissivity was unknown, two thermocouples were attached for the calibration purpose.

As previously mentioned, a thermal elastoplastic finite element numerical model was utilized to assist the development of the new laser welding. The sequentially coupled thermal-mechanical finite element (FE) modeling technique was adopted. Time history of the temperature field was calculated first and the results were then applied as the thermal load in the subsequent mechanical calculation. Because the dimension of the test samples and the fixture was symmetric along the welding pass, only one half of the steel plate was modeled by applying a symmetric boundary condition on the cross-sectional surface of the weld center. The finite element model was constructed by 8-node linear brick elements and consisted of about 126,080 elements with finer elements in the weld and the adjacent regions. The temperature-dependent thermo-physical and mechanical properties were collected from various sources. Isotropic strain hardening was assumed. The analysis was carried out with, a general-purpose finite element code enhanced with welding specific user subroutines.

In the heat transfer finite element analysis, the heat input of the primary welding beam was applied as a double-ellipsoidal volumetric heat source. The ellipsoidal parameters, as well as the absorption coefficient of laser energy, were determined by comparing the simulated weld bead melt zone cross-sectional dimensions to that of the actual experimental welds produced by the primary welding beam only. The

approach used for modeling the heat transfer of the auxiliary beam was different from the primary welding beam. Since melting is not anticipated to occur from the auxiliary heat source, the heat input of the auxiliary beam was modeled as a circular surface heat flux. The accuracy of the circular heat flux used in the numerical model was verified through comparison with thermocouple and IR temperature readings taken during the actual experimental welds. In the mechanical finite element analysis, the translational and rotational displacements of the bottom surface were fully constrained since the 304L sample plates used for the experimental tests were welded to a rigid backing plate during testing (Figure 21).

Due to the unknown surface emissivity of the 304L materials tested in this study, IR and thermocouple thermal data was gathered and compared to calibrate the temperature measurement (Figure 22). The measured data was fitted to a polynomial curve to implicitly represent the surface emissivity (IR intensity vs. temperature relation). It was also found that the surface condition within the region of interest (ROI) had negligible change after welding. Therefore, the fitting curve was further used to calculate the actual temperature throughout the ROI.

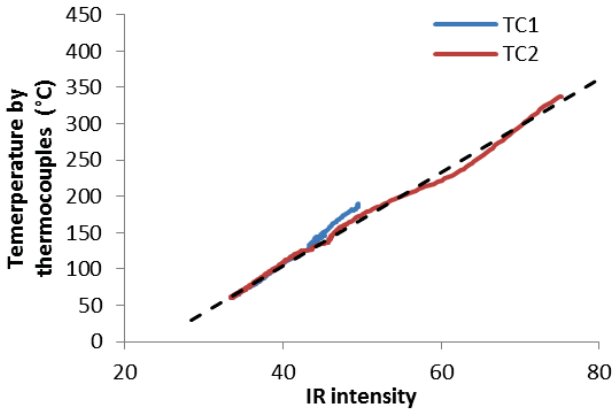

Figure 22: Calibration curve between IR intensity and actual temperature

The comparison of measured vs. simulated evolutions of temperature and transverse strain (perpendicular to welding direction) curves at various distances from the fusion line are plotting in figures shown in the Appendix. Each experimental measurement was repeated by three times. Overall, the simulated results were consistent to the experiments.

With the experimentally validated model, the comparison of transverse stress evolution during cooling among different welding cases is shown in Figure 23. It reveals that higher auxiliary beam power with appropriate scanning pattern was more effective on stress reduction during on-cooling portion of the weld cycle. Patterns a and b (2 kW scan power) were most effective towards producing compressive stress in the critical helium bubble growth temperature range (i.e., greater than 1100 K).

These results constitute the development and validation of a patent-pending technology that intends to proactively manage the stresses during laser repair welding of highly irradiated reactor internals without helium induced cracking. The technology development relied on Integrated Computational Welding Engineering (ICWE) simulations that made it possible to refine and optimize an innovative welding concept and to identify specific process conditions achieving significant stress compression near the weld pool.

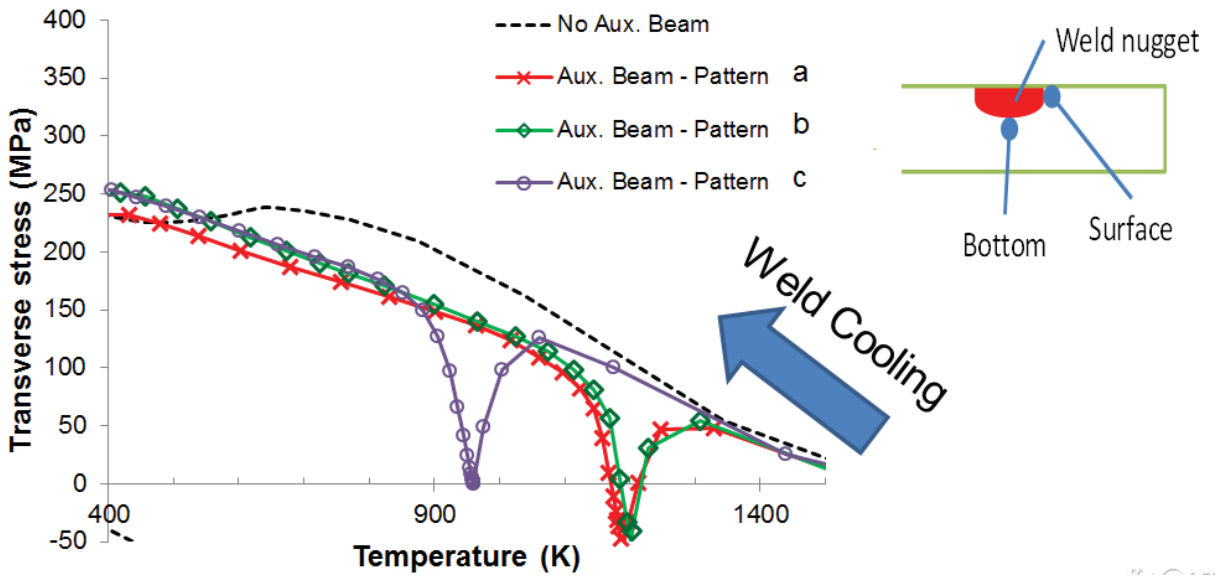

Figure 23: On-cooling FEA transverse stresses, bottom HAZ location only

The candidate welding process conditions identified by the ICWE simulations were experimentally tested with a laser welding system purposely designed and engineered to incorporate the proactive stress management concept. The FEA predicted strain and temperature data agreed with the experimental measurements, indicating the validity of the numerical approach, and the computational modeling data confirmed that the new laser welding approach is able to control the temperature and stress distribution during welding and effectively reduce the tensile stress during the cooling cycle of the weld. As such, this technology is well positioned for initial trials on irradiated materials.

6. Software Quality Assurance Process

As a Department of Energy national laboratory, ORNL has prime contract-imposed mandates and expectations for the Laboratory's overall quality assurance (QA) program. These are contained in DOE Order 414.1D, Quality Assurance for most activities and in DOE Rule 10 CFR 830, Subpart A, Nuclear Safety Quality Assurance Requirements which is imposed on the balance of ORNL activities associated with nuclear facilities, radiological areas, and programs and activities that have the potential to impact nuclear or radiological safety. To meet these requirements, ORNL implements its QA Program Description (PD) which serves as the highest tier QA document for the site. The QAPD provides for addressing sponsor requirements through either the imposition of a QA program based on the ANSI/ISO/ASQ(E) Q9001:2008 standard – for which ORNL is registered - or on an alternate recognized standard.

ORNL has implemented a decades-long nuclear R&D-focused QA program that is described in ORNL document # QAP-ORNL-NR&D-01, Quality Assurance Plan for Nuclear Research and Development Activities Conducted at the Oak Ridge National Laboratory. For the wide-ranging technical activities conducted under the auspices of this plan, the invoked QA requirements are based on two US domestic quality standards: the ASME NQA-1-2008 standard, including the NQA-1a-2009 addendum, entitled Quality Assurance Requirements for Nuclear Facility Applications and the current version of US Nuclear

Regulatory Commission's (NRC) QA requirements defined in 10 CFR 50 Appendix B entitled Quality Assurance Criteria for Nuclear Power Plants and Fuel Reprocessing Plants.

Additionally, the Laboratory's nuclear R&D QA approach implements ASME NQA-1-2008, Part IV, Subpart 4.2, Guidance on Graded Application of Quality Assurance for Nuclear Related Research and Development as the guiding document to tailor the application of quality requirements to each nuclear R&D activity, its associated risks, work phase – basic, applied or development, and the nature of both the planned and potential uses of the final deliverables.

Based on these factors, a number of QA subject areas associated with current and future friction stir welding activities have received emphasis as a part of the work planning and control process:

- Establishing test materials pedigree and maintaining traceability throughout irradiation, test preparation, conduct, and materials storage/archiving.
- Defining and documenting the design of friction stir welding equipment configuration.
- Fully defining material processing planning, testing, and related work controlling documents that are needed to support planned technical activities.
- Controlling the purchase of quality-impacting items and materials to be used.
- Identifying equipment that will require calibration.
- Identifying the records set necessary to fully substantiate how work was performed.
- Software QA.

Software QA is a strong area of emphasis because of the need to ensure that the software that controls the welding process is fully functional and documented to achieve consistent repeatable stir welding results. Software QA also has longer-term considerations associated with the importance of successful results to nuclear industry stakeholders and the anticipated scrutiny of this new process by the NRC.

ORNL maintains a software QA program that mandates that software with potential significant impact to research results must be evaluated and documented to the level necessary to support our deliverables. Specifically this requires that the inputs to the software be fully verified as appropriate and correct for the planned activity, that the software outputs are correct in ensuring a correctly-functioning stir welding process, and that the associated configuration management/control approach ensures that a robust version control process is in place so that the version of the software used for each stir weld completed is known and documented as a part of the processing records.

In pursuit of a strong software QA stance in support of this work, ORNL has contracted with Dynamic Design Solutions (DDS), Inc. to provide the software QA documentation to support verification, validation, and version control. DDS is the organization that is responsible for the design and development of the friction stir welding software. This documentation was due for completion and transmittal to ORNL on April 4, 2017, but its delivery was re-scheduled twice because of operational difficulties experienced by DDS. A draft copy of the documentation was provided by DDS on June 30, 2017, and is currently undergoing review and approval at ORNL.

7. Summary

The development of advanced welding technologies with the potential for enabling repair of highly irradiated stainless steel and nickel-base alloys without helium induced cracking and a facility that would enable the direct testing of these technologies on irradiated materials has represented a significant research and development, as well as facility development, effort. Several challenges have been overcome, and this effort has reached its final phase prior to welding irradiated materials. Installation of

the welding cubicle and supporting systems is nearing completion. Initial FSW and LBW process parameters for use on irradiated materials have been identified. Post-weld evaluation plans are being finalized, and the software quality assurance process is progressing. Completion of these items will allow for the start-up of research and development efforts on irradiated materials in a unique facility that has the potential to be a major long-term asset for researchers and industry stakeholders in the mission to extend the operating lifetimes of existing nuclear reactors.

Acknowledgements

The authors gratefully acknowledge the program management of Keith Leonard, the facility development effort of Scott White and personnel of the Radiochemical Engineering Development Center, and the assistance of Kurt Smith, Richard Howard, Clay Morris, and Rick Lowden, all of Oak Ridge National Laboratory.

References

[1] Miller, R.G., Kinney, K., Feng, Z., Status report on welding hot cell enclosure fabrication, U.S. Department of Energy, Office of Nuclear Energy, Light Water Reactor Sustainability Program, Milestone Report, June 2014.

[2] Tang, W., Feng, Z., Peterson, A.G., Frederick, G.J., et al, Friction-stir cladding and welding process development in welding hot cell environment on unirradiated stainless steels, U.S. Department of Energy, Office of Nuclear Energy, Light Water Reactor Sustainability Program, Milestone Report, June 2015.

[3] Feng, Z., Tang, W., Miller, R.G., Gibson, B.T., et al., Report on the installation of the integrated welding hot cell at Oak Ridge National Laboratory building 7930, U.S. Department of Energy, Office of Nuclear Energy, Light Water Reactor Sustainability Program, Milestone Report, June 2016.

[4] Feng, Z., Cetiner, N., Hu, X., Miller, R.G., et al., Provide documentation on the information and status of both the first and second series of neutron irradiate series of B-doped steels for the weld validation testing to begin in FY17, U.S. Department of Energy, Office of Nuclear Energy, Light Water Reactor Sustainability Program, Milestone Report, Sept 2016.

[5] Tang, W., Gibson, B.T., Feng, Z., Clark, S.R., et al., Report detailing friction stir welding process development for the hot cell welding system, U.S. Department of Energy, Office of Nuclear Energy, Light Water Reactor Sustainability Program, Milestone Report, Sept 2016.

[6] Gibson, B.T., Tang, W., Peterson, A.G., Feng, Z., et al., Evaluating the potential for remote in-process monitoring of tool wear in friction stir welding of stainless steel, *Journal of Manufacturing Science and Engineering*, Accepted for publication.

[7] Sorenson, C.D., Friction stir welding tool designs, *Welding Fundamentals and Process*, Vol 6A, ASM Hand Book, ASM International, 2011, pp. 664 - 667.

[8] Sutton, M.A., Orteum, J.J., Schreier, H.W., Image correlation for shape, motion and deformation measurement, Springer, New York, 2009.

[9] Chen, J., Yu, X., Miller, R., Feng, Z., In situ strain and temperature measurement and modelling during arc welding, *Science and Technology of Welding and Joining*, Vol 20, No 3 (2015) pp. 181 - 188.

Appendix

Comparison of measured vs. simulated evolutions of LBW temperature and transverse strain curves

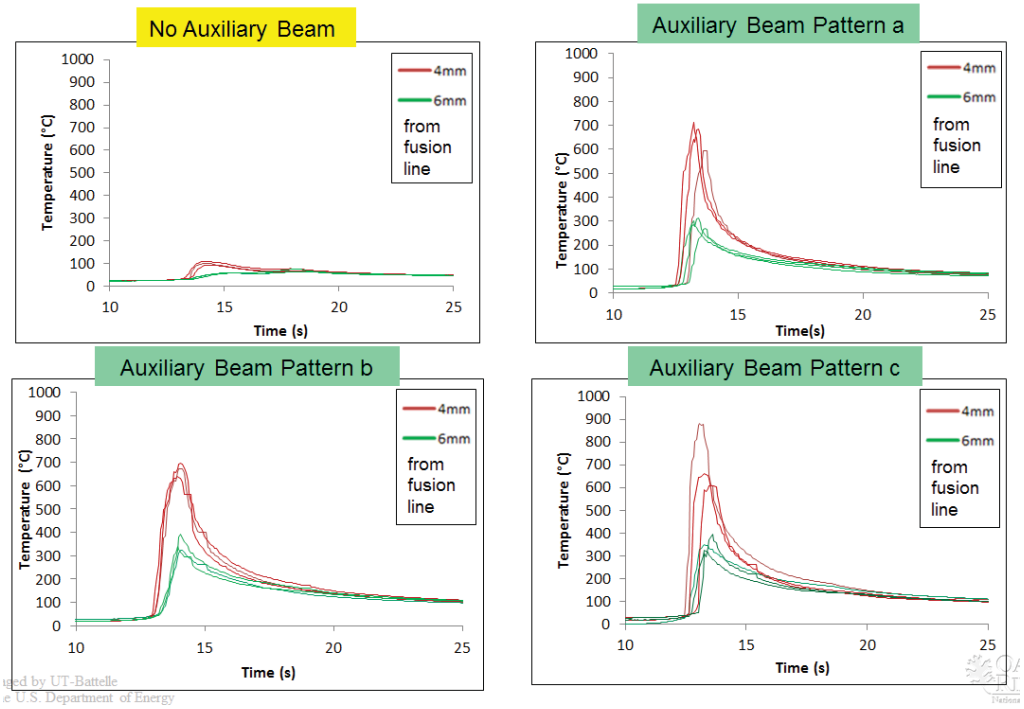

Measured temperature evolutions at varying distances from the fusion line

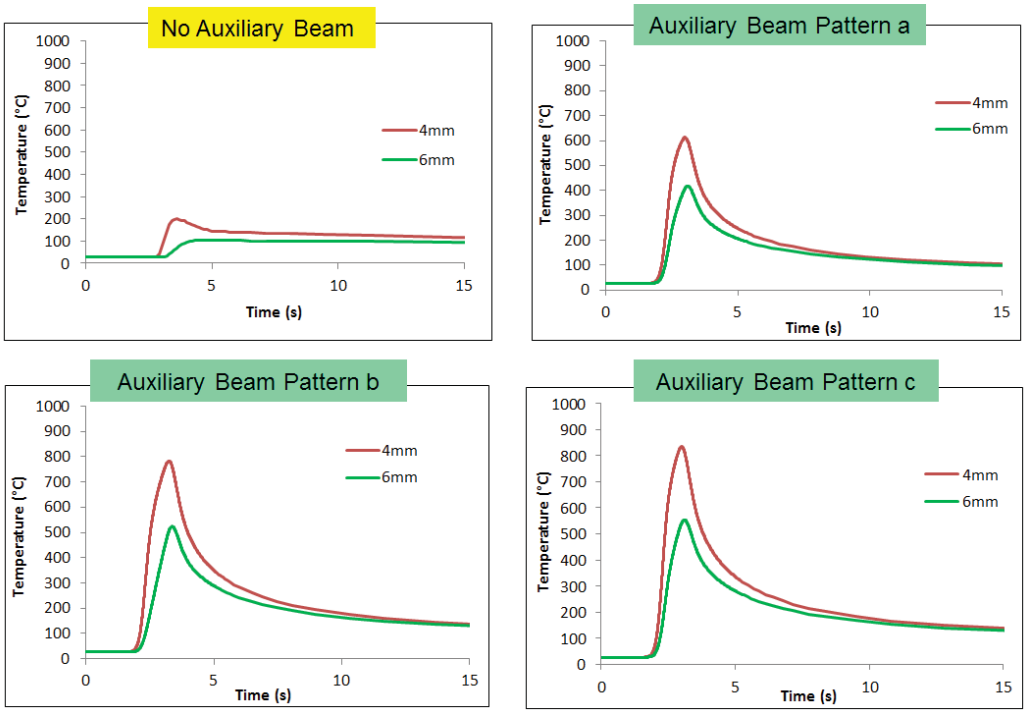

Simulated temperature evolutions at varying distances from the fusion line

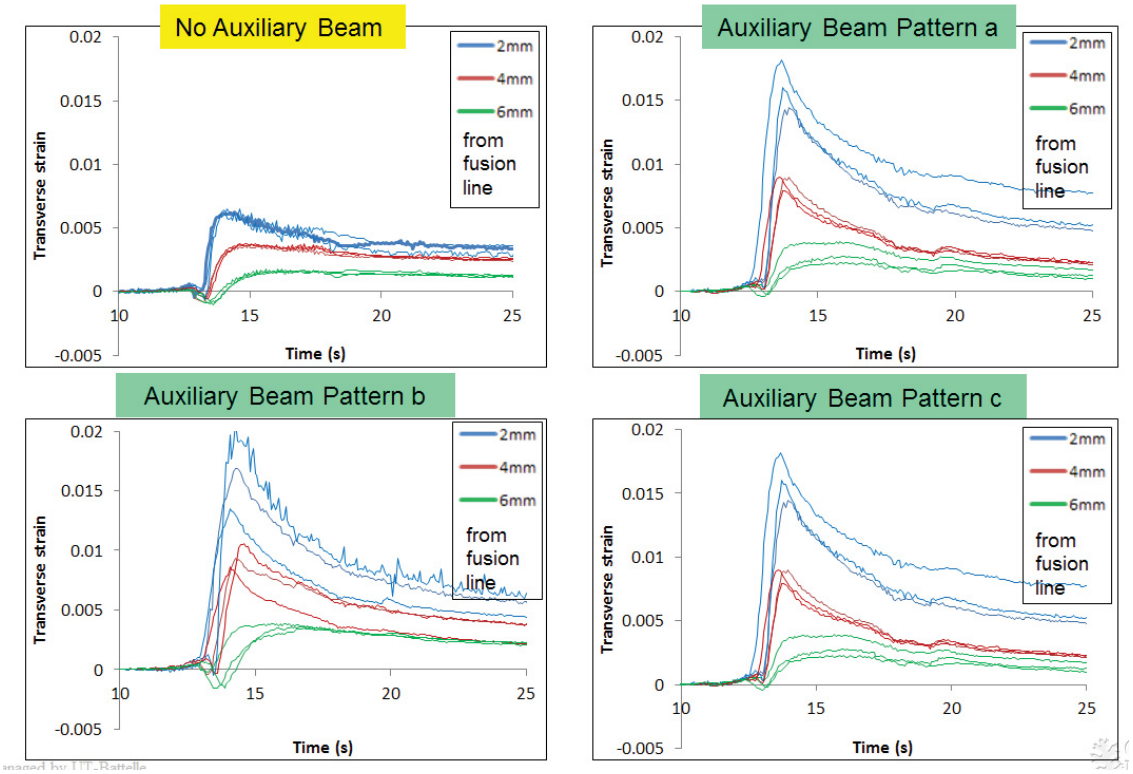

Measured transverse strain evolutions at varying distances from the fusion line

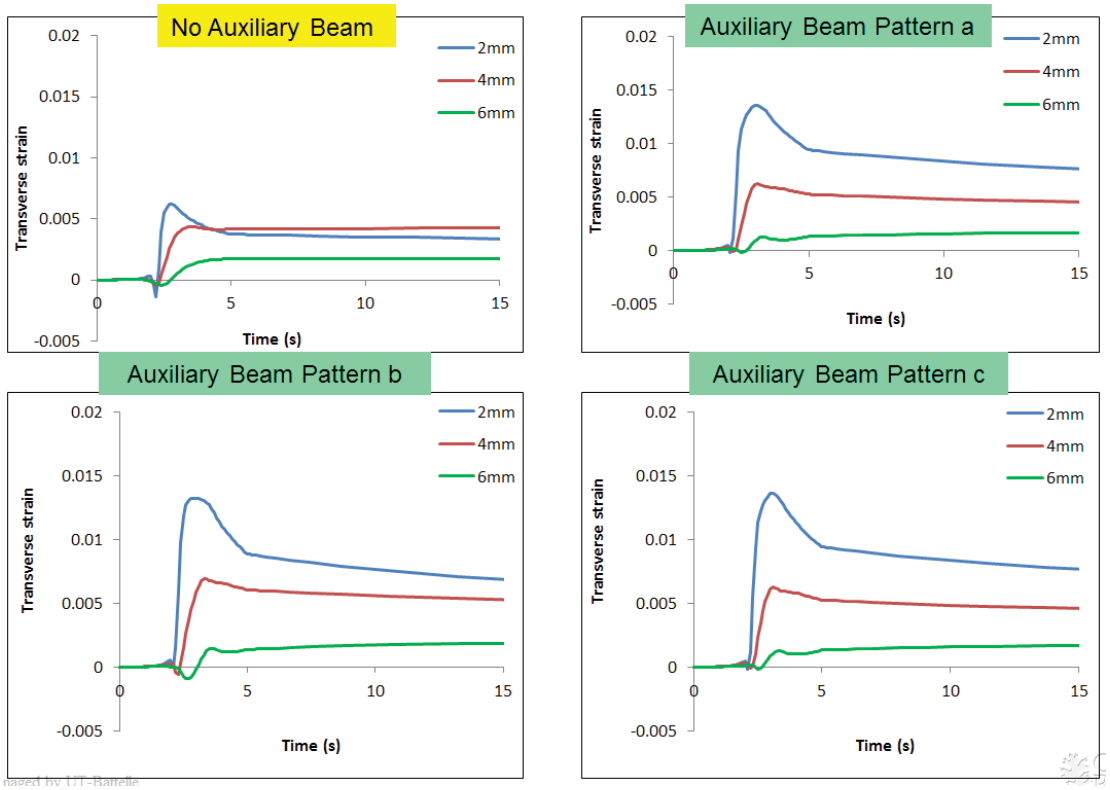

Simulated transverse strain evolutions at varying distances from the fusion line